Published in final edited form as:
Cytoskeleton (Hoboken). 2012 January ; 69(1): 59–69. doi:10.1002/cm.21002.

Plus-end Directed Myosins Accelerate Actin Filament Sliding by Single-headed Myosin VI

Bhagavathi Ramamurthy[1], **Wenxiang Cao**[2], **Enrique M. De La Cruz**[2], and **Mark S. Mooseker**[1,3,4]

[1]Department of Molecular, Cellular and Developmental Biology, Yale University, New Haven, CT

[2]Department of Molecular Biophysics and Biochemistry, Yale University, New Haven, CT

[3]Department of Cell Biology, Yale University, New Haven, CT

[4]Department of Pathology, Yale University, New Haven, CT

Abstract

Myosin VI (Myo6) is unique among myosins in that it moves toward the minus (pointed) end of the actin filament. Thus to exert tension on, or move cargo along an actin filament, Myo6 is working against potentially multiple plus (barbed)-end myosins. To test the effect of plus-end motors on Myo6, the gliding actin filament assay was used to assess the motility of single-headed Myo6 in the absence and presence of cardiac myosin II (Myo2) and myosin Va (Myo5a). Myo6 alone exhibited a filament gliding velocities of 60.34 +/− 13.68 nm/s. Addition of either Myo2 or Myo5a, at densities below that required to promote plus-end movement resulted in an increase in Myo6 velocity (~100-150% increase). Movement in the presence of these plus-end myosins was minus-end directed as determined using polarity tagged filaments. High densities of Myo2 or Myo5a were required to convert to plus-end directed motility indicating that Myo6 is a potent inhibitor of Myo2 and Myo5a. Previous studies have shown that two-headed Myo6 slows and then stalls in an anchored state under load. Consistent with these studies, velocity of a two headed heavy mero myosin form of Myo6 was unaffected by Myo5a at low densities, and was inhibited at high Myo5a densities.

Introduction

Myosin VI (Myo6) is the only known myosin that moves toward the minus (pointed)- end of the actin filament [Wells et al., 1999]. The “reversal” of Myo6 directionality is mediated by a unique calmodulin (CaM) binding insert in the motor domain that structurally reverses the power stroke of the neck-tail domain toward the minus-end of the filament [Menetrey et al., 2005]. Myo6 is widely expressed in metazoan animal species and insights into its numerous cellular functions have been elucidated through studies in *Drosophila, C. elegans*, sea urchin and vertebrates. These functions include cell fate determination, inner ear hair cell function and differentiation, Golgi organization, clathrin-mediated endocytosis, regulated trafficking of membrane proteins such as the cystic fibrosis transduction regulator and EGF receptor, tumor cell migration and regulation of transcription [Ameen et al., 2007; Buss and Kendrick-Jones, 2008; Buss and Kendrick-Jones, 2011; Cheney, 1998; Chibalina et al., 2010; Chibalina et al., 2009]. As the sole minus-end directed myosin, Myo6 must work on actin filament arrays with which potentially large ensembles of plus-end motors are also interacting. For example, the actin cytoskeleton which underlies and supports the apical

Address Correspondence to: Mark S. Mooseker, MCD-Biology, 352 KBT, 219 Prospect St, Yale University, New Haven, CT 06520-8103, mark.mooseker@yale.edu, 203-432-3469.

brush border (BB) cytoskeleton of the intestinal epithelial cell contains at least a dozen plus-end motors (Myo1a,c,e [Tyska et al., 2005],and d [Benesh et al., 2010], Myo2 [Mooseker et al., 1978], Myo5a [Heintzelman et al., 1994], Myo5b [Muller et al., 2008], Myo7a [Bement et al., 1994; Wolfrum et al., 1998], Myo7b [Chen et al., 2001], Myo9b and Myo10 [Bement et al., 1994] in addition to Myo6 [Heintzelman et al., 1994]. The potential functional synergy between Myo6 and plus-end motors is underscored by the effect of loss of the major plus-end motor exerting plus-end force on the BB membrane, Myo1a. In the BB, Myo6 is found at the base of microvilli, associated with the intermicrovillar membrane, sites of clathrin-mediated endocytosis. In the Myo1a knock-out mouse, the association of Myo6 with the BB cytoskeleton is lost [Tyska et al., 2005].

Myo6 purified from tissue is single headed [Lister et al., 2004], although dimerization can be effected by numerous binding interactions including actin binding [Park et al., 2006] and cargo binding to the tail domain [Phichith et al., 2009; Spink et al., 2008]. Single-headed Myo6 is a relatively high duty ratio motor [De La Cruz et al., 2001; O'Connell et al., 2007; Sakata et al., 2007] and two-headed Myo6 is processive, with a duty ratio of ~1 [De La Cruz et al., 2001; Nishikawa et al., 2002; Rock et al., 2001]. Myo6 has a much greater step size than expected for a neck domain/lever arm consisting of just one IQ motif [Rock et al., 2001]. Several studies have demonstrated that the unfolding/lengthening of the three-helix domain in the proximal tail [Mukherjea et al., 2009; Spink et al., 2008], and/or the relatively stiff helical medial tail domain [Sivaramakrishnan et al., 2009] serve to extend the length of the lever arm, resulting in large, but variable step sizes. Recent studies by Liu et al. [2011] have implicated a role for CaM in the extension of the three helix proximal tail domain. Laser trap studies have demonstrated that load has a profound effect on the mechanochemical properties of two-headed Myo6. Increasing load slows Myo6 stepping without altering step size, until the motor stalls at high load, converting it into a stable "anchor" state [Altman et al., 2004; Chuan et al., 2010]. Recently, Ali et al. [2011] analyzed the movement of quantum dots containing both Myo6 and Myo5a. They observed a "tug of war" between the two motors, with the stepping rate of both motors slowed by the resistive load of the other. Thus the action of multiple plus-end motors "tugging" on the same filament, on which Myo6 is working, could have important effects on its motor properties and functions. Moreover, single-headed Myo6 could respond quite differently from two-headed molecules to plus-end load since the cooperative effects of tension between the two heads of a dimeric motor are absent.

In this study we have directly tested the effect of plus-end motors on the *in vitro* filament gliding motility of multiple single-headed Myo6 motors. Surprisingly, given the studies summarized above for effects of load on Myo6, we observed that in the presence of low densities of the plus-end motors, Myo2 or Myo5a, Myo6 velocities were up to 100-150% faster. The converse was not true. Myo6 had a potent inhibitory, braking effect on both Myo2 and Myo5a -mediated gliding filament velocities. No enhancement of velocity by Myo5a was observed for two-headed Myo6 heavy mero myosin (HMM). The increase in single headed, Myo6 velocity requires active, cycling plus-end motors since the non-cycling, "dead head" motor N-ethylmaleimide (NEM) modified -skeletal muscle myosin subfragment 1 (S1) is a potent inhibitor of Myo6 motility.

Results

Full length human Myo6 is single headed

EDC crosslinking of human Myo6 (25 μg/ml) resulted in the formation of several ~ 140-170 kDa bands presumably corresponding to Myo6 heavy chain with 0-2 crosslinked CaM light chains. There is also a very faint high molecular weight band at the top of the gel which may correspond to crosslinked aggregates formed from the > 250kDa bands seen in the absence

of EDC crosslinking. In contrast, EDC crosslinking of Myo5a (25 μg/ml) produced a very high molecular "fuzzy" band resulting from Myo5a heavy chain cross linking to each other and to variable numbers of associated light chains (Fig. 1). There was no detectable 190 kDa Myo5a heavy chain after EDC crosslinking.

In vitro motility properties of Myo5a, cardiac muscle Myo2 and Myo6

One potential problem with assessing the motile properties of a mixture of Myo6 and plus-end motors is that some gliding filaments could be propelled predominantly by either plus- or minus-end directed motors as determined by their relative concentrations and affinity for actin. Thus we first examined effects of plus-end motors on Myo6 motility in the presence of either Myo2 or Myo5a at densities that were below the threshold necessary to yield motility by either Myo2 or Myo5a alone. Gliding filament velocities as a function of motor density (expressed as the concentration of motor used to coat the motility chamber surface) revealed that this threshold was 0.13 μM for cardiac muscle Myo2. The cardiac Myo2 preparations used exhibited a marked reduction in velocity at densities just above that required to support movement, the expected result for a low duty ratio myosin [O'Connell et al., 2007]. Lower threshold densities for mouse cardiac Myo2 have been reported by Szcesna-Cordary et al. [2007]; however, these studies included methyl cellulose in the motility chamber. Although all the studies reported here were in the absence of methyl cellulose, we did observe robust, albeit slower motility of Myo2 at lower densities in the presence of methyl cellulose (0.08μM, 0.3+/− 0.07 um/s; 0.04μM, 0.25 +/− 0.05 um/s).

The threshold concentration of the Myo5a preparation was 12 nM (Fig. 2B) whether purified from frozen or fresh brain tissue. This is a higher threshold density of Myo5a compared to that observed by Mehta et al. [1999]. Nevertheless, the Myo5a in the preparation used exhibited near maximum velocities at the lowest densities that supported movement indicating that the Myo5a used in these studies exhibited motility characteristic of a high-duty ratio motor. The maximum velocity of Myo5a observed is comparable to previously published values [Cheney et al., 1993; Mehta et al., 1999].

The threshold concentration of baculovirus-expressed human Myo6 was ~ 0.007 μM Fig 2C). The velocity of Myo6 propelled movement was essentially constant over the range of concentrations that supported actin filament gliding. Optimal motility with respect to numbers of filaments moving/field was 0.014 μM and this concentration was used for all subsequent assays examining the effect of plus-end motors on Myo6 motility.

The threshold concentration of porcine Myo6 HMM was ~ 0.07 μM (Fig. 2D). As for full length Myo6, the velocity remained relatively constant across the range of motor densities tested. The threshold Myo6 HMM concentration was ~ 10 fold higher than that for full length Myo6. This is presumably due to the absence of the distal portion of the tail domain which may act as a strut that elevates the motor domain of full length Myo6 off the chamber surface. Indeed, chambers containing directly adsorbed porcine Myo6 S1 truncated at the end of the IQ domain (which was quite active based on ATPase) did not support filament gliding (results not shown).

Low densities of cardiac muscle Myo2 and Myo5a increase the filament gliding velocity of single headed Myo6 but not that of two-headed Myo6 HMM

The velocity of Myo6 mediated filament gliding was tested in the presence of a range of Myo2 and Myo5a concentrations below and above the thresholds of plus-end motor required for motility in the absence of Myo6. The data in Fig. 3 are based on assays performed on multiple days using a single Myo6 preparation stored at −20°C in glycerol, multiple freshly thawed aliquots of a liquid nitrogen-frozen Myo5a preparation, and multiple freshly

prepared preparations of cardiac muscle Myo2. Velocities are normalized to the percent difference between motility of Myo6 alone versus that in the presence of Myo2 or Myo5a. This normalization was performed because the velocity of Myo6 varied from day to day, most likely because of variations in room temperature. . Consistent with this possibility, on those days when the velocity of Myo6 alone was either lower or higher than average, there was also a parallel decrease or increase in the plus-end augmentation of Myo6 velocity on that day.

Chamber coating concentrations of 0.014 μM Myo6 and 0.2-50 nM Myo2 all exhibited increased velocity compared to Myo6 alone, with an optimal increase in velocity of ~ 100% increase at a coating concentration of 0.5 nM, although the fold increase in velocity was quite variable over a broad range of Myo2 coating concentrations from 0.2-20 nM. In chambers coated with the Myo2 concentrations above the threshold concentration required for Myo2 motility, gliding velocities decreased to ~ 0 (-77% on the graph in Fig. 3A). At the highest concentrations of Myo2 tested (above 6 μM), the quality of motility was quite poor, with respect to the numbers of filaments moving/field and the duration of movement for those filaments that move. At these Myo2 densities we were unable to score filaments that moved a minimum of 5 frames. Scoring filaments that moved less than 5 frames gave velocities that were up to 6 fold higher than Myo6, but at still significantly slower velocities than that by Myo2 alone (results not shown).

A similar effect of Myo5a on increasing Myo6 mediated gliding velocities was observed (Fig 2B). As for Myo2, inhibition of gliding velocities occurred at concentrations of Myo5a at or above that required for movement in the presence of Myo5a alone. At much higher concentrations, motility resumed, presumably reflective of movements generated by Myo5a only, but as for Myo2, the velocity remained lower than that by Myo5a alone.

To test the effect of low densities of plus-end motor on the motility of two-headed Myo6, the velocity of 0.2μM Myo6 HMM in the presence of low densities of Myo5a was examined. In contrast to full length, single-headed Myo6, two-headed Myo6 HMM velocity was not enhanced by low densities of Myo5a; in most experiments the rates were on average slightly lower than that of Myo6 HMM alone (Fig. 3D). At high Myo5a densities (0.02 μM), at which Myo5a alone supports robust motility, filaments exhibited an unusual, biphasic behavior. Some filaments that land are initially nonmotile but soon after landing the filaments fragment into short filaments that either move away or release from the chamber surface (Supplementary movie 1). Others land and immediately fragment and move away often at rates faster than HMM alone (Supplementary movie 2)-- the reason for the large variation in velocities at high Myo5a coating densities (Fig. #D). This is consistent with the initial Myo5a stalling of HMM motility, which results in a tug of war fragmentation of the filaments which can now be moved either by Myo5a or possibly Myo6. The former is more likely since the velocity of the short fragments is often faster than that of Myo6 HMM alone. We could not verify directionality using polarity tagged filaments (see below) because no two-color polarity tagged filaments survive fragmentation under these conditions.

Polarity tagged filaments were used to verify that the faster moving filaments observed in the presence of low densities of Myo2 or Myo5a were Myo6 dependent, minus end directed movements. In contrast to single color filaments, the quality of motility observed using the polarity tagged filaments was poor with respect to the numbers of two-color filaments moving/field. Moreover, velocities measured for Myo6 both in the absence and presence of plus-end motors were generally slower than that observed using single color filaments. This may be due to the presence of the gelsolin cap on the polarity tagged filaments. Thus collection of sufficient data over the wide range of plus end motor concentrations shown in Fig. 3 was not technically feasible using polarity tagged filaments. Nevertheless, at densities

of Myo2 (Fig 4A) and Myo5 (Fig. 4B) that optimally promote faster motility of Myo6 using single color, uncapped filaments, only minus-end directed filament movements were observed (Supplemental movies 3 and 4). At the highest densities of Myo2 and Myo5a tested, almost no two color filaments survive fragmentation. Consequently only a few filaments, all plus end directed, were observed at these high densities for both Myo2a and Myo5a. However, the range of velocities observed for these few filaments was slower than for either Myo2 or Myo5a in the absence of Myo6. This indicates that Myo6 is a potent inhibitor of Myo2 and Myo5a motility. As noted above, we were unable to observe movement of polarity tagged filaments using Myo6 HMM in the presence of Myo5a. The polarity tagged filaments were fragmented and lost immediately upon landing even at low Myo5a densities.

The range of filament velocities seen at optimal potentiating concentrations of Myo2 and Myo5a using single color filaments indicate that there was no overlap between velocities measured in the absence and presence of either plus-end directed motor (Fig 5). Consistent with the observations obtained with polarity tagged filaments this indicates that the increase in velocity is not due to an averaging of rates of filaments moved by Myo6 and the rates of filaments moved by the faster plus-end motors.

ATP-independent actin filament tethering by NEM-S1 inhibits Myo6 motility

To determine if the increase in single-headed Myo6 motility requires the action of active, cycling plus-end motors, we tested the effect of non-cycling NEM treated muscle myosin S1, which locks onto the actin filament in a rigor-like state in the presence of ATP. At low NEM-S1 coating densities, no increase in Myo6 velocity was observed and at higher concentrations, movement was inhibited partially (7.7 nM) or completely blocked (19 nM; Fig 6). The relatively high concentration of NEM S1 required to inhibit motility of rhodamine phalloidin tagged filaments is likely due to the presence of high densities of unlabeled “black” actin in the motility chamber which will act as a sink for NEM S1

Discussion

The results presented here demonstrate that the velocity of single-headed Myo6, but not two-headed Myo6 HMM is significantly increased in the presence of the plus- end directed motors, cardiac Myo2 and brain Myo5a. We demonstrate that the increased velocity observed in the presence of plus-end motors is not due to an averaging of velocities of filaments moved by Myo6 and those moved by the faster cardiac Myo2 or Myo5a. This is based on the demonstration that the filament movements are minus-end directed when tested at optimal plus-end motor densities using polarity tagged filaments (Fig. 4). Measurement of velocities at optimal plus-end motor densities using the more robustly motile single color filaments, for which many more measurements can be made, also revealed complete lack of slower Myo6 velocities.(Fig. 5). The observed increase in Myo6 velocity is likely due to the plus-end tension generated on the actin filaments undergoing Myo6 directed minus-end movement rather than a direct interaction between Myo6 and either cardiac Myo2 or Myo5a. This is because the observed plus-end motor mediated increase in velocity occurs at low, substoichiometric amounts of both plus-end motors.

The results presented here are in dramatic contrast to results of analogous studies assessing the effects of combined actions of plus-and minus-end motors on microtubule (MT) motility. In the presence of both dynein and kinesin, MTs move significant distances in one direction and then switch directions, with velocities in both the plus- and minus end directions reduced relative to that by each motor alone [Vale et al., 1992]. Similarly, the velocities of the plus-end kinesin, kinesin-5 was inhibited by increasing densities of the minus-end kinesin, Ncd, and vice versa with short back and forth MT movements occurring at “the

balance point" between these two motors [Tao et al., 2006]. A somewhat different "tug of war" was observed for movement along actin filaments of quantum dots containing both Myo5a and two-headed Myo6 [Ali et al., 2011]. Under these conditions Myo5a "wins" the tug of war most of the time, but stepping rates for both Myo5a and Myo6 are slowed due to resistive load imparted by the opposing motor. These elegant studies are consistent with previous studies showing that two-headed Myo6 slows and finally stalls into an anchored state under increasing optical trap-imposed load [Altman et al., 2004; Chuan et al., 2010]. Moreover, the failure of Myo5a to potentiate motility of two headed Myo6 HMM suggests that there is a fundamental difference in the response of single versus double headed Myo6 to load. This striking difference in response to load could result from co-operative mechanical interactions between the two heads that affect the duty cycle - e.g. by inhibiting ADP release from the trailing head [Altman et al., 2004; De La Cruz et al., 2001].

There are at least three possible mechanisms by which plus-end motor load on the actin filament could increase the velocity of single-headed Myo6, none of which is mutually exclusive of the others. However, for the reasons indicated, there are problems with all of these possible mechanisms. First, plus-end tension could increase the ATPase cycle rate, perhaps through increasing the rate of ADP release—the rate-limiting step in Myo6 ATPase cycle [De La Cruz et al., 2001]. Arguing against this possibility is that studies on two-headed Myo6 show the opposite effect of load on ATPase activity and velocity [Altman et al., 2004]. Addition of comparably low ratios of cardiac Myo2 had no effect on actin-activated ATPase of Myo6 as assayed in solution (unpublished observations) but unlike Myo6 motors in the motility chamber, Myo6 was not anchored to the substrate. Unfortunately, attempts to measure Myo6 ATPase activity in motility chambers were unsuccessful due to the very low levels of ATP hydrolysis under optimal gliding motility conditions (0.014 μM Myo6 surface coating concentration and 10 nM F-actin). Second, plus-end motor tension on the actin filament might result in a lengthening and/or stiffening of the proximal/medial tail portion of the Myo6 lever arm resulting in an increase in step size. This could result from tension-mediated unfolding of the 3-helix domains in the proximal tail [Liu et al., 2011; Mukherjea et al., 2009] and/or a "stiffening" of the junction between the proximal tail and the single ER/K alpha helix in the medial tail domain [Spink et al., 2008]. However, it is important to note that increasing optical trap load does not increase the step size of two headed Myo6 [Altman et al., 2004; Chuan et al., 2010]. Also, one might expect that the resistive load generated by NEM-S1 to have a similar effect on neck/tail structure— unless on/off cycling of the load is required. In this regard it would be interesting to see how two headed Myo6 would respond to on/off oscillating optical trap load. A third mechanism is that plus-end motor tension propagates a change in the actin filament helix, resulting in a filament substrate that is more favorable for Myo6 stepping. Effects of substoichiometric myosin binding on the dynamics of actin filament structure are consistent with potential contributions originating from myosin-linked changes in actin filament structural dynamics. For example, Kozuka et al. [2006] measured fluorescence resonance energy transfer (FRET) between actin subunits and observed that the actin helix oscillates between "open" and "closed" states, with the closed state exhibiting higher levels of energy transfer. Moreover, in the presence of Myo5a, the rate of oscillation was significantly reduced, and the open state was stabilized. However, this possibility is countered by the studies of Prochniewicz et al. [2010] who observed that muscle myosin S1 and Myo5a binding have opposite effects on intrafilament subunit torsion, with S1 decreasing and Myo5a increasing rates of intrafilament subunit movement. In both cases, these effects display non-nearest neighbor (i.e. long-range) cooperativity such that they affect distal filament subunits without bound myosin. Moreover these changes accelerate Myo5a binding and slow S1 binding to partially decorated filaments with changes in binding occurring roughly on the same scale as changes in motility observed here. One possible explanation how long range effects of both Myo5a and Myo2 on actin filament structure

could promote faster Myo6 velocity is that the studies of Prochniewicz et al. [2010] were performed in solution while our studies both the motors and gliding actin filaments are tethered to the substrate.

One very puzzling aspect of the results presented here is that increases in Myo6 velocity were observed at even very low substrate densities of both cardiac Myo2 (Fig. 3A) and Myo5a (Fig 3B), even assuming that all the plus end motors added to the chamber were adsorbed and in an orientation which allows interaction with actin filaments. This is particularly surprising for cardiac Myo2 given its low duty ratio. Indeed, to quote of the reviewers of this paper: “As stated in the previous review, I find it incredible that such low densities of Myo2 (which has a low duty ratio) are able to cause a motility affect.” One, albeit speculative possibility, assuming tension-mediated lengthening/stiffening of the tail portion of the lever arm occurs is that the “relaxation” rate of this structural change could be relatively slow. If so, then a Myo6 motor “conformationally charged” by plus-end tension could take multiple larger steps after that tension is released.

With respect to understanding the mechanochemical behavior of Myo6 in the cell, these observations indicate that factors regulating its monomer-dimer state could play critical roles in determining the response of this myosin to resistive load. A single-headed Myo6 motor would tend to move faster along actin filaments that are under plus- end motor tension (with or without bound cargo) while a two-headed Myo6 motor (with or without cargo) may become anchored under plus-end motor tension until that tension is released. For example, two-headed Myo6 motors bound to a clathrin-coated pit might remain tightly bound in an anchored state until load is released upon scission of the coated vesicle by dynamin, allowing Myo6 to deliver the endocytic vesicle to the endosome. On the other hand a single-headed motor might rapidly move off the coated pit prior to vesicle formation. Such differences in monomer versus dimer motor properties in response to load could contribute significantly to the various membrane trafficking functions of Myo6 and the cycling of Myo6 between membrane trafficking compartments.

The only system in which the ratio of Myo6 to plus-end motors has been quantified is in the intestinal BB where the principal plus-end motor associated with the BB membrane is Myo1a. There is ~50 fold more Myo1a than Myo6 [Heintzelman et al., 1994]. However, Myo1a and Myo6 are low and high duty ratio motors respectively. Thus the net opposing forces at steady state might be comparable assuming all available motors are engaged. As noted above, loss of Myo1a from the microvillus in the Myo1a KO results in dissociation of Myo6 from the BB [Tyska et al., 2005]. One possibility is that under significant Myo1a dependent load, the dimeric, anchored state of Myo6 is favored while in its absence single-headed Myo6 prevails, resulting in steady state redistribution of Myo6 from the BB actin cytoskeleton.

Materials and methods

Protein purification

Full-length human Myo6-FLAG and CaM were co-expressed in the baculovirus system and purified as described in Rock et al. [2001]. Porcine, dimeric Myo6 HMM-FLAG truncated at Arg992, which includes the proximal and medial tail domain and a C-terminal leucine zipper dimerization domain was baculovirus expressed and purified as described in Robblee et al. [2004]. The oligomerization state of the expressed human Myo6 was determined by chemical crosslinking of 25 μg/ml Myo6 or Myo5a (as a two headed positive control) with the zero-length crosslinker 1-ethyl-3-(3-dimethylaminopropyl) carbodiimide (EDC) as described in Post et al. [2002).The samples were run on 3-7% SDS PAGE gels, electro-transferred to nitrocellulose and immunoblotted using 0.05 μg/ml rabbit anti Myo6

[Heintzelman et al., 1994] or 0.05 μg/ml rabbit anti Myo5a [Espreafico et al., 1992]. Immunoreactive crosslinked products were visualized using horseradish peroxidase-conjugated secondary antibody (Pierce, Rockford, IL) and enhanced chemo luminescence (GE Healthcare, Piscataway, NJ).

Myo5a was purified from either frozen or freshly dissected chick brain tissue as described in Cheney [1998]. Sucrose (35% w/v) was added to purified Myo5a and 30 μl aliquots were drop frozen in liquid nitrogen, and stored at −80°C. Aliquots were thawed rapidly on the day of the experiment and used in the *in vitro* motility assay.

Myo2 was purified from mouse cardiac tissue using a modification of Kalabokis and Szent-Gyorgyi [1997]. Briefly, adult mouse cardiac tissue was homogenized using a hand held Omni micro homogenizer (Omni International, Kennesaw, GA) in low salt buffer containing 40 mM KCl, 5 mM Imidazole (pH 7.2), 1 mM $MgCl_2$, 5 mM DTT, 0.5 mM EGTA, and 0.1 mM EDTA. The homogenate was clarified and washed 3 times by centrifugation at 10,000 g for 10 min. The resulting pellet was suspended in high salt-ATP buffer (0.6 M KCl, 5 mM Imidazole (pH 7.2), 1 mM $MgCl_2$, 5 mM DTT, 5 mM ATP, 0.2 mM EGTA and 0.1 mM EDTA) and centrifuged at 40,000 g for 15 min. Ammonium sulfate was added to the supernatant to 40% saturation and the resulting pellet discarded. The Myo2 in the 40% supernatant was precipitated by addition of ammonium sulfate to 55% saturation. The 55% Myo2 pellet, which by SDS PAGE contained only Myo2 heavy and light chains, was stored on ice and used within 4 weeks of preparation. The Myo2 preparations as assayed by the method of De La Cruz et al. [2001] exhibited levels of maximal actin activated MgATPase of ~ 6.85 +/− 2.5 /s/head at room temperature.

Skeletal muscle myosin S1 purified from chicken breast muscle Myo2 was treated with N-ethyl maleimide (NEM) as described in Meeusen and Cande [1979]. Frozen aliquots of NEM-S1 were stored at −80°C and thawed for use on the day of the experiment. ATP-independent actin binding of the preparation was assessed by cosedimentation of 3 μM NEM-S1 with 8 μM F-actin in the absence or presence of 2 mM ATP, 10 mM imidazole, pH 7.2, 2 mM $MgCl_2$, 1 mM EGTA, 1 mM DTT. In both the absence and presence of ATP ~ 20% of the total NEM S1 remained in the supernatant after sedimentation indicating that the preparation was ~ 80% active with ~ 20% inactive, presumably denatured protein.

G-actin was purified from chicken breast muscle according to Spudich and Watt [1971]. Purified actin was drop frozen in liquid nitrogen and stored at −80°C in ~30 μl pellets. Pellets were thawed rapidly just before labeling. Alternatively, freshly purified, gel filtered G-actin (a gift from the laboratory of Thomas Pollard, Yale University) was used for labeling.

Protein concentrations were measured using a UV-Vis spectrophotometer (ND-1000 NanoDrop Technologies, Wilmington, DE).

Actin filament labeling

Actin filaments were stabilized with rhodamine phalloidin as described in O'Connell and Mooseker [2003] for use in the *in vitro* motility assay. Rhodamine phalloidin-labeled actin was used up to 4 weeks after labeling. Dual-color, polarity tagged filaments used for directionality measurements were made by two different methods as described in Herm-Gotz et al. [2002] and O'Connell and Mooseker [2003] with slight modifications. In the first method, plus-end capped nuclei were made by polymerization of rhodamine-labeled G-actin (Cytoskeleton Inc., Denver, CO) in the presence of gelsolin and Ca^{2+}. These plus-end capped filaments were stabilized with phalloidin, sheared and used to nucleate actin from the minus ends, followed by labeling with Alexa 488 phalloidin. In the second method, the

plus-end, gelsolin-capped seeds were made with unconjugated actin and labeled with rhodamine phalloidin. Both methods yield two color filaments with the plus-ends labeled red. Polarity tagged actin filaments were prepared fresh for use each day.

In vitro motility assay

The *in vitro* gliding actin motility assay was performed as described in Kron and Spudich [1986]. Motility chambers were constructed as described previously [Post et al., 1998; Post et al., 2002]. The chambers were pre-treated with 10 μg/ml BSA in Buffer A (75mM KCl, 10 mM imidazole (pH 7.2), 2.5 mM $MgCl_2$, 1 mM EGTA). Myosin was added to the chamber and was allowed to incubate for 15′ at RT. This was followed by addition of 1 mg/ml BSA in Buffer A. Inactive myosin heads were blocked by addition of 5 nM unlabeled F-actin. Motility was visualized at 23.4 ± 1°C using labeled actin diluted to a final concentration of 5 nM in motility buffer (20 mM KCl, 10 mM Imidazole (pH 7.2), 2.5 mM $MgCl_2$, 1 mM EGTA, 5 mM DTT, 2 mM Pefabloc, 10 mM MgATP, 400 μg/ml glucose oxidase, 200 μg/ml catalase, 0.3% glucose, 3 μM CaM). For all three myosins used in these studies, the robustness of motility (at motor densities above the threshold for movement using single color filaments) with respect to numbers of filaments moving/field was time dependent. The majority (70-90%) of filaments landing during the first data set/chamber exhibited movement. However, in subsequent fields collected at later time points, the number of nonmotile filaments increased. Thus only 2-3 movies per chamber were made. To determine the absorption efficiency of Myo6 in these chambers, immunoblot analysis of mock chambers washed with Buffer A after incubation with 0.014 μM Myo6 indicated that >90% of the Myo6 remained in the chamber after the wash.

When two motors were included in the experiment, the plus-ended motor was added first, followed by Myo6. Myo5a and Myo6 were diluted in buffer A. Myo2 was added to the chamber in high salt (0.6 M KCl, 5 mM imidazole (pH 7.2), 1 mM $MgCl_2$, 5 mM DTT, 0.2 mM EGTA and 0.1 mM EDTA). Although this order of motor addition was used for the results presented here, in test studies reversing the order of motor incubation gave comparable results. Each myosin was incubated in the chamber for 15 mins at RT. Pre-incubation of control chambers (Myo6 alone) o preincubated with either high salt (for Myo2 experiments) or Buffer A (for Myo5a experiments) for 15 min. prior to addition of Myo6 gave identical results to chambers with no pre-incubation step.

Image acquisition and velocity measurement

Fluorescently labeled actin filament movement was visualized by Nikon TE300 multi-mode epi-fluorescence microscope equipped with CoolSNAP HQ, (Tucson, AZ) CCD camera. Images were acquired using Metamorph v.6.1 (Molecular Devices, Sunnyvale, CA) software. Rhodamine-phalloidin-labeled actin movement was visualized using the red channel and the polarity -tagged actin filaments by using time-lapse, multi-mode emission channel [O'Connell and Mooseker, 2003]. Myo2 and Myo5a mediated actin filament movement was acquired at the rate of 1 frame/3 seconds, Myo6 propelled filament movement was acquired at the rate of 1 frame/10 seconds. Motility in chambers with both Myo6 and either Myo2 or Myo5a was acquired at the rate of 1 frame/10 seconds. Exposure time for all acquisitions was 200 ms.

Velocity was measured using 'track points' function of the Metamorph software, v 6.2r 1 (Molecular Devices, Sunnyvale, CA). To determine velocity, the x-y position of the forward tip of a moving filament was selected in one frame and its position was tracked along subsequent frames. A distribution of multiple lengths of actin filaments was used in velocity measurements to avoid filament-length bias. Measurements were made on both filaments already landed and moving at the start of image acquisition and on filaments that landed and

moved during the the assay. Only filaments moving continuously for 5 consecutive frames were included in the measurements shown in Figs. 2-6.

Supplementary Material

Refer to Web version on PubMed Central for supplementary material.

Acknowledgments

The authors thank Drs. Benjamin Spink and James Spudich, Stanford University for generously providing us with the Myo6 preparation used in this study. We also thank the Pollard laboratory for providing gel filtered G-actin used in preparing polarity-tagged filaments. This work was supported by NIH grants GM 073823 and DK 25387 to MSM and GM097348 to EMDLC. EMDLC is an NSF CAREER award recipient (MCB-0546353), American Heart Association Established Investigator (0940075N), and Hellman Family Foundation Fellow.

References

Ali M, Kennedy G, Safer D, Trybus K, Sweeney H, Warshaw D. Myosin Va and myosin VI coordinate their steps while engaged in an in vitro tug of war during cargo transport. Proc. Natl. Acad Sci (USA)). 2011; 108:E535–E541. [PubMed: 21808051]

Altman D, Sweeney HL, Spudich JA. The mechanism of myosin VI translocation and its load-induced anchoring. Cell. 2004; 116:737–49. see comment. [PubMed: 15006355]

Ameen N, Silvis M, Bradbury NA. Endocytic trafficking of CFTR in health and disease. J Cyst Fibros. 2007; 6:1–14. [PubMed: 17098482]

Bement WM, Hasson T, Wirth JA, Cheney RE, Mooseker MS. Identification and overlapping expression of multiple unconventional myosin genes in vertebrate cell types. 1994; 91:11767.

Benesh AE, Nambiar R, McConnell RE, Mao S, Tabb DL, Tyska MJ. Differential localization and dynamics of class I myosins in the enterocyte microvillus. Mol Biol Cell. 2010; 21:970–8. [PubMed: 20089841]

Buss F, Kendrick-Jones J. How are the cellular functions of myosin VI regulated within the cell? Biochem Biophys Res Commun. 2008; 369:165–75. [PubMed: 18068125]

Buss F, Kendrick-Jones J. Multifunctional myosin VI has a multitude of cargoes. Proceedings of the National Academy of Sciences of the United States of America. 2011; 108:5927–8. [PubMed: 21464329]

Chen ZY, Hasson T, Zhang DS, Schwender BJ, Derfler BH, Mooseker MS, Corey DP. Myosin-VIIb, a novel unconventional myosin, is a constituent of microvilli in transporting epithelia. Genomics. 2001; 72:285–96. [PubMed: 11401444]

Cheney RE. Purification and assay of myosin V. Methods Enzymol. 1998; 298:3–18. [PubMed: 9751866]

Cheney RE, O'Shea MK, Heuser JE, Coelho MV, Wolenski JS, Espreafico EM, Forscher P, Larson RE, Mooseker MS. Brain myosin-V is a two-headed unconventional myosin with motor activity. Cell. 1993; 75:13–23. see comments. [PubMed: 8402892]

Chibalina MV, Poliakov A, Kendrick-Jones J, Buss F. Myosin VI and optineurin are required for polarized EGFR delivery and directed migration. Traffic. 2010; 11:1290–303. [PubMed: 20604900]

Chibalina MV, Puri C, Kendrick-Jones J, Buss F. Potential roles of myosin VI in cell motility. Biochem Soc Trans. 2009; 37:966–70. [PubMed: 19754433]

Chuan P, Spudich JA, Dunn AR. Robust mechanosensing and tension generation by myosin VI. J Mol Biol. 2010; 405:105–12. [PubMed: 20970430]

De La Cruz EM, Ostap EM, Sweeney HL. Kinetic mechanism and regulation of myosin VI. J Biol Chem. 2001; 276:32373–81. [PubMed: 11423557]

Espreafico EM, Cheney RE, Matteoli M, Nascimento AA, De Camilli PV, Larson RE, Mooseker MS. Primary structure and cellular localization of chicken brain myosin-V (p190), an unconventional myosin with calmodulin light chains. 1992; 119:1541–1557.

Heintzelman MB, Hasson T, Mooseker MS. Multiple unconventional myosin domains of the intestinal brush border cytoskeleton. J Cell Sci. 1994; 107(Pt 12):3535–43. [PubMed: 7706404]

Herm-Gotz A, Weiss S, Stratmann R, Fujita-Becker S, Ruff C, Meyhofer E, Soldati T, Manstein DJ, Geeves MA, Soldati D. Toxoplasma gondii myosin A and its light chain: a fast, single-headed, plus-end-directed motor. Embo J. 2002; 21:2149–58. [PubMed: 11980712]

Kalabokis VN, Szent-Gyorgyi AG. Cooperativity and regulation of scallop myosin and myosin fragments. Biochemistry. 1997; 36:15834–40. [PubMed: 9398315]

Kozuka J, Yokota H, Arai Y, Ishii Y, Yanagida T. Dynamic polymorphism of single actin molecules in the actin filament. Nat Chem Biol. 2006; 2:83–86. [PubMed: 16415860]

Kron SJ, Spudich JA. Fluorescent actin filaments move on myosin fixed to a glass surface. Proc Natl Acad Sci U S A. 1986; 83:6272–6. [PubMed: 3462694]

Lister I, Schmitz S, Walker M, Trinick J, Buss F, Veigel C, Kendrick-Jones J. A monomeric myosin VI with a large working stroke. Embo J. 2004; 23:1729–38. [PubMed: 15044955]

Liu, y.; Hsin, J.; Kim, H.; Selvin, P.; Schulten, K. Extension of a three-helix bundle domain of myosin VI and key role of calmodulins. Biophys. J. 2011; 100:2964–2973. [PubMed: 21689530]

Meeusen RL, Cande WZ. N-ethylmaleimide-modified heavy meromyosin. A probe for actomyosin interactions. J Cell Biol. 1979; 82:57–65. [PubMed: 158029]

Mehta AD, Rock RS, Rief M, Spudich JA, Mooseker MS, Cheney RE. Myosin-V is a processive actin-based motor. Nature. 1999; 400:590–3. [PubMed: 10448864]

Menetrey J, Bahloul A, Wells AL, Yengo CM, Morris CA, Sweeney HL, Houdusse A. The structure of the myosin VI motor reveals the mechanism of directionality reversal. Nature. 2005; 435:779–85. [PubMed: 15944696]

Mooseker MS, Pollard TD, Fujiwara K. Characterization and localization of myosin in the brush border of intestinal epithelial cells. J Cell Biol. 1978; 79:444–53. [PubMed: 152766]

Mukherjea M, Llinas P, Kim H, Travaglia M, Safer D, Menetrey J, Franzini-Armstrong C, Selvin PR, Houdusse A, Sweeney HL. Myosin VI dimerization triggers an unfolding of a three-helix bundle in order to extend its reach. Mol Cell. 2009; 35:305–15. [PubMed: 19664948]

Muller T, Hess MW, Schiefermeier N, Pfaller K, Ebner HL, Heinz-Erian P, Ponstingl H, Partsch J, Rollinghoff B, Kohler H, Berger T, Lenhartz H, Schlenck B, Houwen RJ, Taylor CJ, Zoller H, Lechner S, Goulet O, Utermann G, Ruemmele FM, Huber LA, Janecke AR. MYO5B mutations cause microvillus inclusion disease and disrupt epithelial cell polarity. Nat Genet. 2008; 40:1163–5. [PubMed: 18724368]

Nishikawa S, Homma K, Komori Y, Iwaki M, Wazawa T, Hikikoshi Iwane A, Saito J, Ikebe R, Katayama E, Yanagida T, Ikebe M. Class VI myosin moves processively along actin filaments backward with large steps. Biochem Biophys Res Commun. 2002; 290:311–7. [PubMed: 11779171]

O'Connell CB, Mooseker MS. Native Myosin-IXb is a plus-, not a minus- end-directed motor. Nat Cell Biol. 2003; 5:171–2. [PubMed: 12563277]

O'Connell CB, Tyska MJ, Mooseker MS. Myosin at work: motor adaptations for a variety of cellular functions. Biochim Biophys Acta. 2007; 1773:615–30. [PubMed: 16904206]

Park H, Ramamurthy B, Travaglia M, Safer D, Chen LQ, Franzini-Armstrong C, Selvin PR, Sweeney HL. Full-length myosin VI dimerizes and moves processively along actin filaments upon monomer clustering. Mol Cell. 2006; 21:331–6. [PubMed: 16455488]

Phichith D, Travaglia M, Yang Z, Liu X, Zong AB, Safer D, Sweeney HL. Cargo binding induces dimerization of myosin VI. Proc Natl Acad Sci U S A. 2009; 106:17320–4. [PubMed: 19805065]

Post PL, Bokoch GM, Mooseker MS. Human myosin-IXb is a mechanochemically active motor and a GAP for rho. J. Cell Sci. 1998; 111:941–950. [PubMed: 9490638]

Post PL, Tyska MJ, O'Connell CB, Johung K, Hayward A, Mooseker MS. Myosin-IXb is a single-headed and processive motor. J Biol Chem. 2002; 277:11679–83. [PubMed: 11801597]

Prochniewicz E, Chin HF, Henn A, Hannemann DE, Olivares AO, Thomas DD, De La Cruz EM. Myosin isoform determines the conformational dynamics and cooperativity of actin filaments in the strongly bound actomyosin complex. J Mol Biol. 2010; 396:501–9. [PubMed: 19962990]

Robblee J, Olivares A, De La Cruz EM. Mechanism of nucleotide binding to actomyosin VI: evidence for allosteric head-head communication. J.Biol. Chem. 2004; 279:38608–38617. [PubMed: 15247304]

Rock RS, Rice SE, Wells AL, Purcell TJ, Spudich JA, Sweeney HL. Myosin VI is a processive motor with a large step size. Proc Natl Acad Sci U S A. 2001; 98:13655–9. [PubMed: 11707568]

Sakata S, Watanabe Y, Usukura J, Mabuchi I. Characterization of native myosin VI isolated from sea urchin eggs. J Biochem (Tokyo). 2007; 142:481–90. [PubMed: 17846066]

Sivaramakrishnan S, Sung J, Ali M, Doniach S, Flyvbjerg H, Spudich JA. Combining single-molecule optical trapping and small-angle x-ray scattering measurements to compute the persistence length of a protein ER/K alpha-helix. Biophys J. 2009; 97:2993–9. [PubMed: 19948129]

Spink BJ, Sivaramakrishnan S, Lipfert J, Doniach S, Spudich JA. Long single alpha-helical tail domains bridge the gap between structure and function of myosin VI. Nat Struct Mol Biol. 2008; 15:591–7. [PubMed: 18511944]

Spudich JA, Watt S. The regulation of rabbit skeletal muscle contraction. I. Biochemical studies of the interaction of the tropomyosin-troponin complex with actin and the proteolytic fragments of myosin. J Biol Chem. 1971; 246:4866–71. [PubMed: 4254541]

Szcesna-Cordary D, Jones M, Moore J, Watt J, Kerrick W, Wang Y, Wagg C, Lopaschuk G. Myosin regulatory light chain E22K mutation results in decreased cardiac intracellular calcium and force transients. FASEB J. 2007; 21:3974–3985. [PubMed: 17606808]

Tao L, Mogilner A, Civelekoglu-Scholey G, Wollman R, Evans J, Stahlberg H, Scholey JM. A homotetrameric kinesin-5, KLP61F, bundles microtubules and antagonizes Ncd in motility assays. Curr Biol. 2006; 16:2293–302. [PubMed: 17141610]

Tyska MJ, Mackey AT, Huang JD, Copeland NG, Jenkins NA, Mooseker MS. Myosin-1a is critical for normal brush border structure and composition. Mol Biol Cell. 2005; 16:2443–57. [PubMed: 15758024]

Vale RD, Malik F, Brown D. Directional instability of microtubule transport in the presence of kinesin and dynein, two opposite polarity motor proteins. J Cell Biol. 1992; 119:1589–96. [PubMed: 1469050]

Wells AL, Lin AW, Chen LQ, Safer D, Cain SM, Hasson T, Carragher BO, Milligan RA, Sweeney HL. Myosin VI is an actin-based motor that moves backwards. Nature. 1999; 401:505–8. [PubMed: 10519557]

Wolfrum U, Liu X, Schmitt A, Udovichenko IP, Williams DS. Myosin VIIa as a common component of cilia and microvilli. Cell Motil Cytoskeleton. 1998; 40:261–71. [PubMed: 9678669]

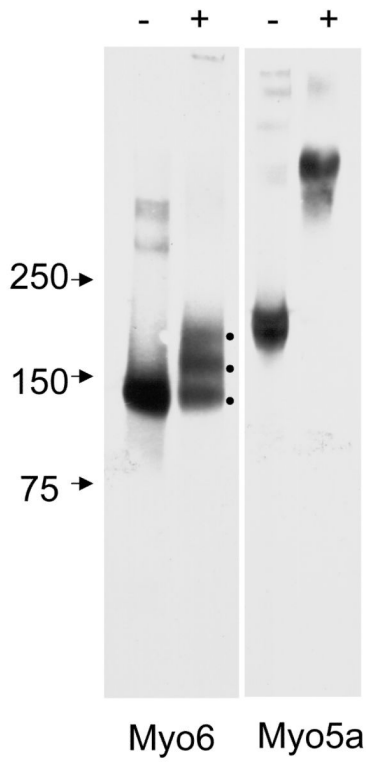

Fig. 1.

EDC crosslinking of human Myo6 and Myo5a. Immunoblot analysis of 25 μg/ml Myo6 and Myo5a without (-) and with (+) EDC crosslinking. Note the three bands in the Myo6 lane after EDC treatment presumably representing Myo6 heavy chain with 0-2 crosslinked CaM light chains. In contrast EDC treatment of Myo5a results in complete loss of monomeric heavy chain and a very high molecular weight smear is present, presumably representing Myo5a heavy chain dimer and variable numbers of light chains.

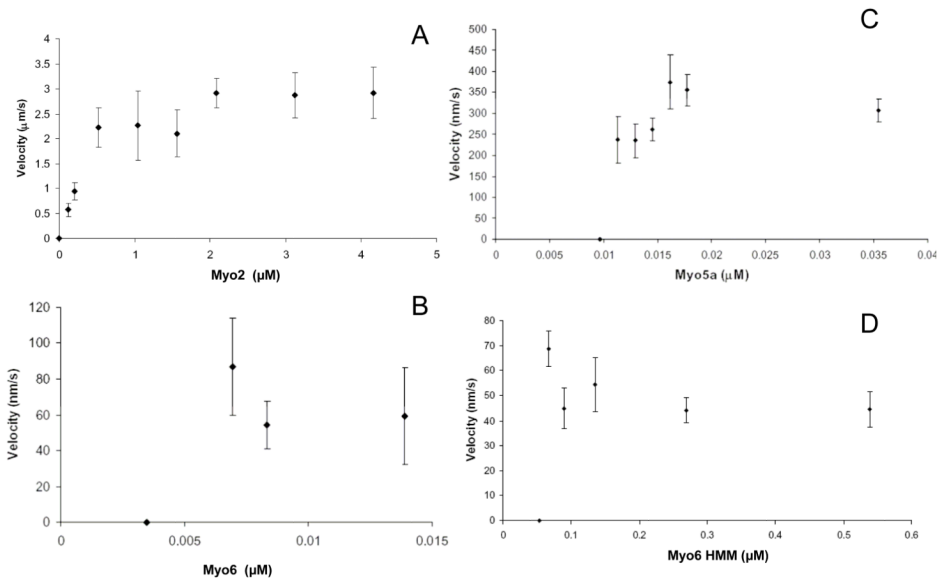

Fig. 2.

Gliding filament velocities of Myo2, Myo5a, Myo6, and Myo6 HMM as a function of motor density. Velocities of rhodamine-labeled actin filaments propelled by directly adsorbed Myo2 purified from mouse cardiac tissue (A)**,** Myo5a purified from chick brain (B)**,** baculovirus expressed Myo6 (C) and Myo6 HMM (D) in the motility assay are shown. The concentrations of myosin used to coat the surfaces of the motility chambers are shown on the x-axes. Filament velocity averages were obtained from a minimum of 2 days of experiments. Values are represented as mean ± SD. The number of filaments for which velocities were measured ranged from 4-23 (A), 5-17 in (B) and 10-20 in (C) and 7-27 in (D).

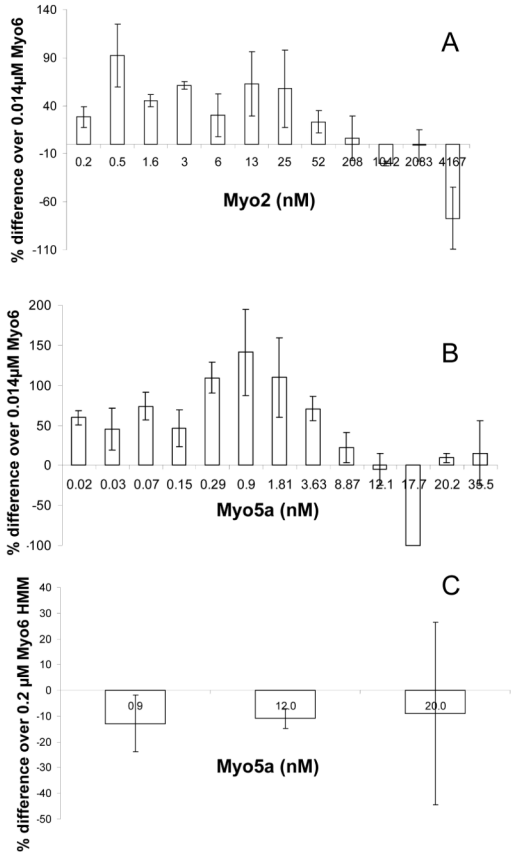

Fig. 3.

Single headed Myo6, but not Myo6 HMM velocity increases in the presence of plus-end directed motors. (A,B). Percentage change (relative to Myo6 alone) in gliding velocity of filaments by 0.014 μM Myo6 with the addition of Myo2 (A),Myo5a (B) is shown as a function of adsorption concentration of either Myo2 or Myo5a. (C). Motility of 0.2μM Myo6 HMM in the presence of increasing concentrations of Myo5a. Motility of either 0.014 μM Myo6 or 0.2 μM Myo6 HMM in the absence of plus-end motor on each day was considered baseline. Bars indicate average of percent-differences obtained from 2-3 days of experiments in (A and C) and 2-4 days of experiments in (B). Values are expressed as average ± SD. Number of filaments for which velocities were measured ranged from 10-66 in (A), 30 – 127 in (B) and 9-67 in (C).

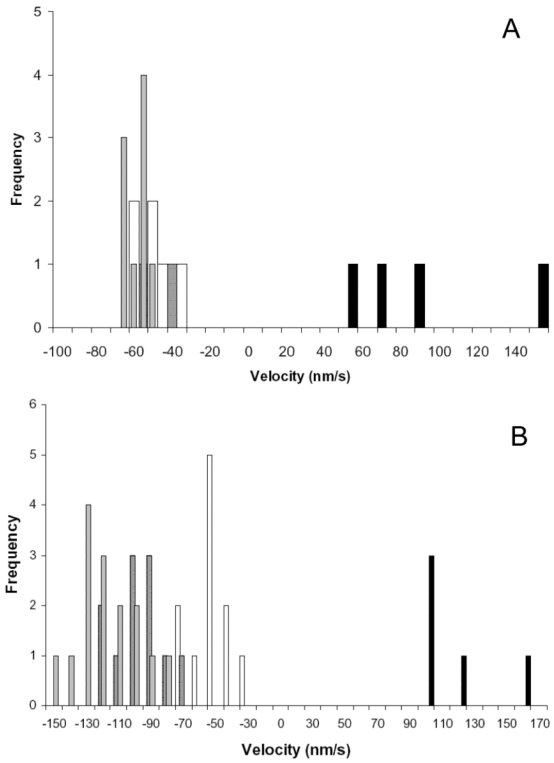

Fig. 4.

Myo6 motility is minus-end directed in the presence of Myo2 (A) and Myo5a (B). (A) Velocity distribution of two-color polarity tagged filaments by 0.014μM Myo6 in the absence (open bars) and presence of 0.5nM (hatched bars), 125 nM (gray bars) and 2.0 μM (black bars) Myo2 is shown. (B). Velocity distribution of polarity tagged filaments in the absence of Myo5a (open bars) and presence of 0.17 nM (hatched bars), 0.93 nM (grey bars) and 37 nM (black bars) Myo5a is shown. For (A) and (B) negative and positive numbers on the x-axis indicate minus-end and plus-end movement of filaments respectively. Only at high densities of Myo2 or Myo5a were plus-end directed movements observed.

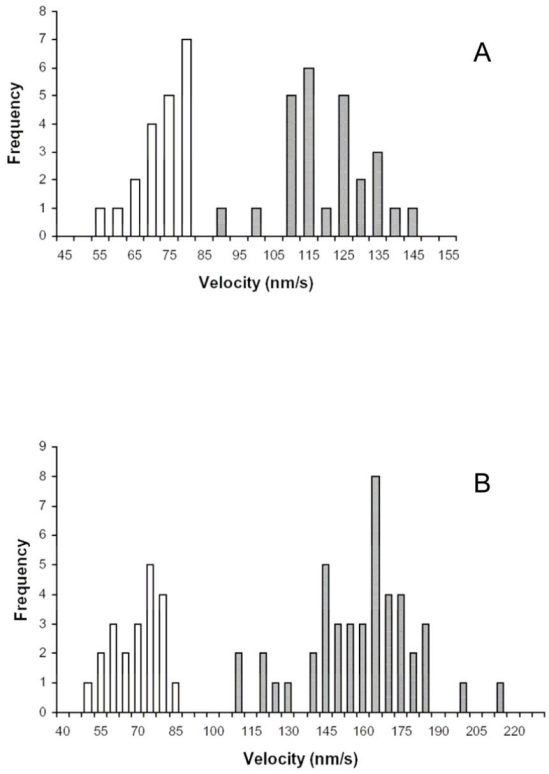

Fig. 5.

Distribution of velocities for Myo6 in the absence and presence of plus-end myosins at Myo2 (A) and Myo5a (B) concentrations that exhibit maximum increases in Myo6 motility. Gliding velocities as a function of number of filaments observed by 0.014 μM Myo6 in the absence (open bars) or presence (hatched bars) of either 0.5 nM Myo2 (A) or 0.9 nM Myo5a (B) are shown. Note that there is no overlap in velocities in the absence and presence of plus-end motor, indicating that the increased velocities is not an average of slower Myo6-minus end movement and faster plus-end motor mediated movement.

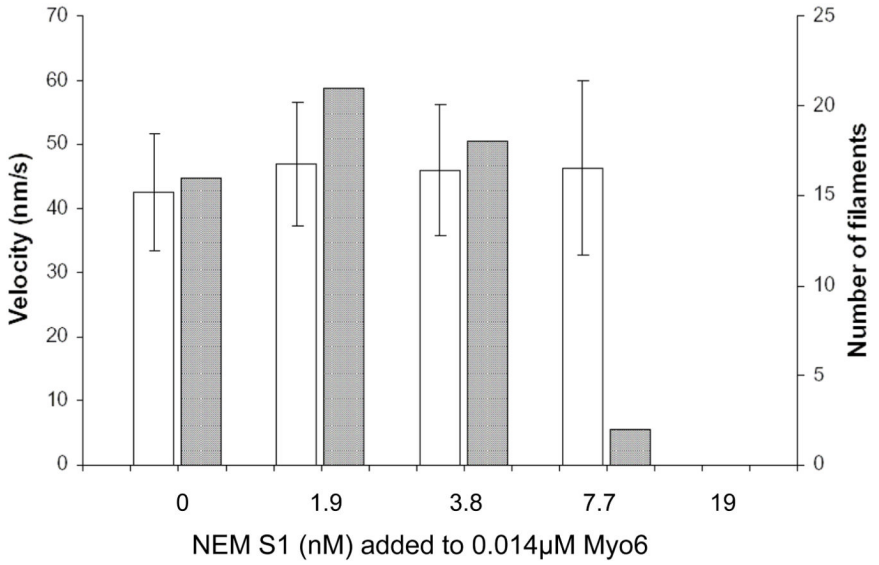

Fig. 6.

NEM S1 does not increase Myo6 velocity. The histogram depicts velocity (open bars) and number (grey bars) of landing filaments moved by 0.014 μM Myo6 in the absence and presence of NEM S1. Values in the open bars are represented as mean ± SD. No increases in velocities are observed and at the higher NEM-S1 concentrations but movement is inhibited with respect to numbers of filaments moving (7.7 nM), and then completely blocked (19 nM).